Direct Numerical Observation of Anomalous Diffusion in Random Media

Victor Pham and Michael W. Deem
Chemical Engineering Department, University of California, Los Angeles, CA 90095-1592
mwdeem@ucla.edu

We present computer simulations of anomalous diffusion, $\langle r^2(t)\rangle \sim at^{1-\delta}$, in two dimensions. The Monte Carlo calculations are in excellent agreement with previous renormalization group calculations. Interestingly, use of a high quality pseudo-random number generator is necessary to observe the anomalous diffusion. A linear-feedback, shift-register method leads to incorrect, super-diffusive motion of the random walkers.

82.20.Db, 05.40.+j, 82.20.Mj

1. INTRODUCTION

Certain types of physically realizable disorders cause anomalous sub-diffusion in two dimensions [1,2]. In these unusual cases the mean square displacement of random walkers does not increase linearly with time, but rather increases sub-linearly with time, $\langle r^2(t)\rangle \sim at^{1-\delta}$. The exponent for this scaling is continuously variable in the strength of disorder. In fact, the exponent can be found exactly for the type of singular Gaussian disorder that leads to sub-diffusion [3–8]. This special disorder corresponds physically to quenched, charged defects. The defects can either be true, electrostatic charges or topological "charges." In either case, the quenched charges interact with the moving particles of interest via a long-range, logarithmic potential.

Diffusion in a variety of random media has been considered by numerical simulation. Typical disorders that have been investigated include non-singular potential disorder [9], random fluid flows [10–12], fractal media [13–15], optical molasses [16], and topologically disordered structures [17]. The random walk Monte Carlo simulation method is used in most numerical studies of diffusion. To date, however, there are no numerical studies that verify the renormalization group predictions of anomalous diffusion in singular, two-dimensional, random potential fields. Preliminary results were cited in the review by Bouchaud and Georges [18], but a formal publication did not ensue.

This same type of quenched, "ionic" disorder subjects chemical reactions to transport limitations and causes anomalous kinetic behavior. Two dimensions is particularly interesting, since this is also the upper critical dimension for bimolecular reactions [19–22], in addition to being the upper critical dimension for the charged disorder. The kinetics of chemical reactions, of course, have always been a subject of interest for scientists and engineers. In most cases, the reactant diffusion is normal, and the effect of diffusion limitations on the rate of chemical reaction is easy to calculate. Anomalous diffusion, however, leads to anomalous kinetics. In this case, the effect on the rate of chemical reaction is not so widely known. The kinetics of the reactions $A+A \rightarrow \emptyset$, $A+B \rightarrow \emptyset$, and $A^+ + B^- \underset{\tau}{\overset{\lambda}{\rightleftharpoons}} AB$ in singular disorder have been derived analytically [21–23]. In these references, a field-theoretic treatment of anomalous kinetics was worked out, and renormalization group predictions were derived. These studies show that the reactions become transport limited in the long time regime. At long times, where the diffusion is anomalous, the kinetics also becomes anomalous.

Simulations to test these theoretical predictions would be of great interest. A necessary prerequisite for proceeding with these numerical studies of anomalous kinetics is first the ability to simulate anomalous diffusion. This ability requires both constructing the disorder and performing the diffusive motion in the quenched disorder.

In this article, we present numerical observations of anomalous diffusion in two dimensions using the Monte Carlo method. In section 2 we discuss the appropriate form of the quenched disorder. In section 3 we introduce our method for creating the random potential and for simulating motion in this potential. Our results are presented in section 4. A discussion of the results is presented in section 5, where a comparison is made with the renormalization group predictions. We conclude in section 6.

2. THE QUENCHED DISORDER

We consider the motion of one charged particle in a sea of quenched charges in two dimensions. The statistics of the motion of the particle is completely determined by the statistics of the quenched potential field that the particle encounters. The quenched charges, which obey bulk charge neutrality, give rise to a charge-charge correlation function that vanishes as k^2 for small k in Fourier space. The potential, which is the convolution of the charge distribution with the logarithmic Coulomb law, gives rise to a potential-potential correlation function that diverges as $1/k^2$ for small k [24]. This long-ranged correlation function for the potential experienced by the diffusing particle is exactly of the form that leads to anomalous diffusion.

In two dimensions the interaction between the charges and the diffusing particle, and between the quenched

charges themselves, is logarithmic. Electrostatic charges in two dimensions, or line charges in three dimensions, interact with this law. Certain topological defects in two dimensions also interact with this same law. For example, dislocations in solids interact with a logarithmic law due to induced long-range elastic strain fields. Disclinations in hexatic membranes also interact with this effective law, due to screening of the induced strain fields by free dislocations. Typical examples of these topological defects include line defects in three dimensional crystals, vortices in superfluids, and flux lines in superconductors [25].

The exponent for the mean square displacement depends indirectly on the density of defects via the prefactor of the potential-potential correlation function. The form of correlation function appropriate for small k is $\hat{\chi}_{vv}(k) \sim \gamma/k^2$, where γ is the strength of the disorder, and $\hat{\chi}_{vv}(\mathbf{k}) = \int d^d\mathbf{r} \exp(i\mathbf{k}\cdot\mathbf{r})\chi_{vv}(\mathbf{r})$ is the Fourier transform of the correlation function. We are free to chose different behavior away from the origin in Fourier space. A natural choice for this correlation function is the inverse of the diffusive Green's function. On a square lattice with spacing Δr we, thus, use the form

$$\hat{\chi}_{vv}(\mathbf{k}) = \frac{\gamma(\Delta r)^2}{4 - 2\cos(k_x\Delta r) - 2\cos(k_y\Delta r)} \ . \tag{1}$$

Note that this form of $\hat{\chi}_{vv}(k)$ has the appropriate limiting behavior as the lattice spacing become infinitesimally small and as the wavelength becomes large. The particles move through this potential field starting from random initial positions. Renormalization group calculations have rather convincingly shown that the mean square displacement exhibits an anomalous behavior at long times [1–8,26]. On a log-log scale, the mean square displacement as a function of time has a slope of $1 - \delta$, where

$$\delta = \left[1 + \frac{8\pi}{\beta^2\gamma}\right]^{-1} \tag{2}$$

and $\beta = 1/(k_BT)$.

3. SIMULATION METHOD

We now consider the creation of the Gaussian random potential $V(\mathbf{r})$ on a lattice. The potential takes on real values at each lattice site. The probability of observing any specific potential distribution is given by

$$P[V] = \frac{e^{-\beta H[V]}}{Z} \ , \tag{3}$$

where

$$\begin{aligned}\beta H[V] &= \frac{1}{2}\int d^d\mathbf{r}d^d\mathbf{r}' V(\mathbf{r})\chi_{vv}^{-1}(\mathbf{r}-\mathbf{r}')V(\mathbf{r}') \\ &= \frac{1}{2}\int \frac{d^d\mathbf{k}}{(2\pi)^d}|\hat{V}(\mathbf{k})|^2\hat{\chi}_{vv}^{-1}(\mathbf{k}) \\ &= \frac{1}{2}\sum_{\mathbf{k}}\frac{(\Delta k)^d}{(2\pi)^d}|\hat{V}(\mathbf{k})|^2\hat{\chi}_{vv}^{-1}(\mathbf{k}) \ ,\end{aligned} \tag{4}$$

Z is a normalizing constant, and $\Delta k = 2\pi/(N\Delta r)$. Here the lattice is in d dimensions ($d = 2$ in our case), has N unit cells on a side, and has lattice spacing Δr. The Fourier transform is given by $\hat{V}(\mathbf{k}) = \int d^d\mathbf{r}V(\mathbf{r})\exp(i\mathbf{k}\cdot\mathbf{r}) = \sum_{\mathbf{r}}(\Delta r)^d V(\mathbf{r})\exp(i\mathbf{k}\cdot\mathbf{r})$. Since $\hat{V}(-\mathbf{k}) = \hat{V}^*(\mathbf{k})$, we have

$$\beta H = \sum_{\mathbf{k}_{1/2}}\sigma(\mathbf{k})\left(\frac{\Delta k}{2\pi}\right)^d|\hat{V}(\mathbf{k})|^2\hat{\chi}_{vv}^{-1}(\mathbf{k}) \tag{5}$$

with $\mathbf{k}_{1/2}$ meaning half of k space and

$$\sigma(\mathbf{k}) = \begin{cases} 1/2, & \text{if } \mathbf{k} \text{ is on a special point} \\ \\ 1, & \text{otherwise} \end{cases} \ , \tag{6}$$

where the special points are the origin, the corners of the lattice, and the intersections of k_x-axis and k_y-axis with the lattice boundaries. In this form, $\hat{V}(\mathbf{k})$ and $\hat{V}(\mathbf{k}')$ are independent as long as $\mathbf{k} \neq \mathbf{k}'$. The potential $\hat{V}(\mathbf{k})$ is Gaussian with the following variance for the real and imaginary components for $\mathbf{k}$ not special

$$\left\langle\left[\mathrm{Re}\hat{V}(\mathbf{k})\right]^2\right\rangle = \frac{1}{2}\Omega\hat{\chi}_{vv}(\mathbf{k}) \tag{7}$$

$$\left\langle\left[\mathrm{Im}\hat{V}(\mathbf{k})\right]^2\right\rangle = \frac{1}{2}\Omega\hat{\chi}_{vv}(\mathbf{k}) \ , \tag{8}$$

where $\Omega = (N\Delta r)^d$ is the volume of the system. If $\mathbf{k}$ is special,

$$\mathrm{Im}\hat{V}(\mathbf{k}) = 0 \ , \tag{9}$$

and

$$\left\langle\left[\mathrm{Re}\hat{V}(\mathbf{k})\right]^2\right\rangle = \Omega\hat{\chi}_{vv}(\mathbf{k}) \ . \tag{10}$$

Also, by definition, $\hat{V}(\mathbf{0}) = \int d^d\mathbf{r}V(\mathbf{r})$. Since it is not the actual magnitude of the potential but rather its gradient that is of interest, we define $V' = V - \langle V\rangle$. In this form, $\hat{V}'(\mathbf{0}) = 0$ and $\nabla V' = \nabla V$. We use the potential V' in the simulation. To create the potential $V'(\mathbf{r})$ that we need, we first create $\hat{V}'(\mathbf{k})$ in half of k-space by generating independent Gaussian random numbers with variances given by Eqs. (7)-(10). We then generate the other half of k-space using the relation $\hat{V}'(-\mathbf{k}) = \hat{V}'^*(\mathbf{k})$. Finally, we generate V' in real space by performing an inverse fast Fourier transform [27].

Alternatively, we can construct a real potential by first generating a complex $V(\mathbf{r})$ and then extracting a real potential, $V'(\mathbf{r})$. Specifically, we generate a complex Gaussian field with the probability distribution

$$P[V] = Z^{-1} \exp\left[- \int d^d\mathbf{r} d^d\mathbf{r}' V^*(\mathbf{r}) \chi^{-1}(\mathbf{r}-\mathbf{r}') V(\mathbf{r}') \right] . \tag{11}$$

Note that the fields $\mathrm{Re}V(\mathbf{r})$ and $\mathrm{Im}V(\mathbf{r})$ are each Gaussian. Thus, we find

$$\langle V^*(\mathbf{r}) V(\mathbf{r}') \rangle = \chi(\mathbf{r}-\mathbf{r}'). \tag{12}$$

We define

$$V'(\mathbf{r}) = \mathrm{Re}V(\mathbf{r}) + \mathrm{Im}V(\mathbf{r}). \tag{13}$$

$V'(\mathbf{r})$ is also Gaussian, since

$$\begin{aligned} & \int d^d\mathbf{r} d^d\mathbf{r}' V^*(\mathbf{r}) \chi_{vv}^{-1}(\mathbf{r}-\mathbf{r}') V(\mathbf{r}') \\ = & \int d^d\mathbf{r} d^d\mathbf{r}' \mathrm{Re}V(\mathbf{r}) \chi_{vv}^{-1}(\mathbf{r}-\mathbf{r}') \mathrm{Re}V(\mathbf{r}') \\ + & \int d^d\mathbf{r} d^d\mathbf{r}' \mathrm{Im}V(\mathbf{r}) \chi_{vv}^{-1}(\mathbf{r}-\mathbf{r}') \mathrm{Im}V(\mathbf{r}') \\ - & i \int d^d\mathbf{r} d^d\mathbf{r}' \mathrm{Im}V(\mathbf{r}) \chi_{vv}^{-1}(\mathbf{r}-\mathbf{r}') \mathrm{Re}V(\mathbf{r}') \\ + & i \int d^d\mathbf{r} d^d\mathbf{r}' \mathrm{Re}V(\mathbf{r}) \chi_{vv}^{-1}(\mathbf{r}-\mathbf{r}') \mathrm{Im}V(\mathbf{r}'). \end{aligned} \tag{14}$$

The complex part of the above equation vanishes, since $\chi_{vv}^{-1}(\mathbf{r}-\mathbf{r}') = \chi_{vv}^{-1}(\mathbf{r}'-\mathbf{r})$ for a medium obeying Eq. (1). From our definition of V', we find

$$\langle V'(\mathbf{r}) V'(\mathbf{r}') \rangle = \chi_{vv}(\mathbf{r}-\mathbf{r}'). \tag{15}$$

This definition of V' leads to a real, Gaussian potential field with the correct statistics. It is, therefore, an equally valid quenched random potential.

With the potential established, we shift focus to the initial conditions for the particle and the mechanics for diffusion. In the theoretical treatment of anomalous diffusion, the particles are assumed to be uniformly distributed over the lattice. In our simulation, therefore, we choose the initial positions of the random walkers from a uniform distribution. In addition, we also examine the case of a Boltzmann distribution of initial positions, as would be appropriate, for example, for a NMR experiment on an equilibrated system. The particles are selected from a random initial position on a finite lattice, and they begin to diffuse at $t = 0$. We could let one particle diffuse an infinitely long time and record its behavior exactly as prescribed by theory. Depending on whether the diffusion is self-averaging, we may also need to average over different realizations of the potential. Unfortunately, lattice effects will appear at long times as a result of the periodic boundary conditions. Another method, which is more efficient and yields better statistics, is to sample many random walkers for a shorter period of time. This will work as long as the observation time is long enough to be in the scaling region, that is, as long as the system is large enough. We have investigated finite size effects and found that a square lattice of $N = 2048$ unit cells on a side is sufficiently large to allow the particles to be in the scaling regime for our range of parameter values. At short times, the particles will display normal diffusion behavior. At intermediate times, the diffusivity will tend to zero. At long times, we will observe the anomalous sub-diffusion, where $\langle r^2(t) \rangle$ is expected to be proportional to $t^{1-\delta}$ as $t \to \infty$.

The statistics of the random walk on the lattice are conveniently described by a master equation. This master equation defines the probabilities and rates of all possible hops that the random walker can execute. We exactly solve this master equation by a Poisson process [28]. In one dimension, the master equation looks like

$$\frac{dP_n}{dt} = U_{n-1}P_{n-1} - D_nP_n + D_{n+1}P_{n+1} - U_nP_n, \tag{16}$$

where P_n is the probability for being at site x_n at time t, U_n is the rate at which transitions occur from x_n to x_{n+1} and D_n is the rate at which transitions occur from x_n to x_{n-1}. In a two dimensional space, we denote the rates by $\tau_{n,m}^{(1)}$, $\tau_{n,m}^{(2)}$, $\tau_{n,m}^{(3)}$, and $\tau_{n,m}^{(4)}$, where $\tau_{n,m}^{(1)}$ and $\tau_{n,m}^{(2)}$ are rates at which transitions occur from $x_{n,m}$ to $x_{n+1,m}$ and $x_{n-1,m}$ respectively, and $\tau_{n,m}^{(3)}$ and $\tau_{n,m}^{(4)}$ are rates at which transitions occur from $x_{n,m}$ to $x_{n,m+1}$ and $x_{n,m-1}$ respectively. The two dimensional master equation is

$$\begin{aligned} \frac{dP_{n,m}}{dt} = & \tau_{n-1,m}^{(1)} P_{n-1,m} - \tau_{n,m}^{(1)} P_{n,m} \\ & + \tau_{n+1,m}^{(2)} P_{n+1,m} - \tau_{n,m}^{(2)} P_{n,m} \\ & + \tau_{n,m-1}^{(3)} P_{n,m-1} - \tau_{n,m}^{(3)} P_{n,m} \\ & + \tau_{n,m+1}^{(4)} P_{n,m+1} - \tau_{n,m}^{(4)} P_{n,m}. \end{aligned} \tag{17}$$

We demand that this master equation lead to a Boltzmann distribution of the random walkers at long times. In other words, we want the stationary probability P_n^S of being at site $x_{n,m}$ to be

$$P_n^S = \frac{(\Delta r)^2 e^{-\beta V(x_{n,m})}}{Z}. \tag{18}$$

This distribution will arise if detailed balance is enforced. For example, the condition of detailed balance for transitions in the x direction is

$$\tau_{n+1,m}^{(2)} P_{n+1,m} = \tau_{n,m}^{(1)} P_{n,m} \ . \tag{19}$$

This criterion implies, with the use of the Boltzmann distribution,

$$\frac{P_{n+1,m}}{P_{n,m}} = \frac{\tau_{n,m}^{(1)}}{\tau_{n+1,m}^{(2)}} = e^{-[\beta V(x_{n+1,m}) - V(x_{n,m})]} \ . \tag{20}$$

Hence, one consistent expression for the rates $\tau^{(1)}_{n,m}$ and $\tau^{(2)}_{n,m}$ is

$$\tau^{(1)}_{n,m} = \frac{D}{(\Delta r)^2} e^{\beta[V(x_{n,m})-V(x_{n+1,m})]/2} \tag{21}$$

$$\tau^{(2)}_{n,m} = \frac{D}{(\Delta r)^2} e^{\beta[V(x_{n,m})-V(x_{n-1,m})]/2} \ . \tag{22}$$

Similar relations hold for the transition rates in the y direction:

$$\tau^{(3)}_{n,m} = \frac{D}{(\Delta r)^2} e^{\beta[V(x_{n,m})-V(x_{n,m+1})]/2} \tag{23}$$

$$\tau^{(4)}_{n,m} = \frac{D}{(\Delta r)^2} e^{\beta[V(x_{n,m})-V(x_{n,m-1})]/2} \ . \tag{24}$$

We use these transition rates to generate a stochastic Poisson process. Specifically, a particle begins at a site $x_{n,m}$. The particle waits at this site with an exponentially distributed amount of time characterized by its mean value

$$\langle dt \rangle = \frac{1}{\tau^{(1)}_{n,m} + \tau^{(2)}_{n,m} + \tau^{(3)}_{n,m} + \tau^{(4)}_{n,m}} \ . \tag{25}$$

We generate the actual time increment via

$$dt = -\frac{1}{\tau^{(1)}_{n,m} + \tau^{(2)}_{n,m} + \tau^{(3)}_{n,m} + \tau^{(4)}_{n,m}} \ln(x) \ , \tag{26}$$

where x is uniformly distributed random number with $0 < x \leq 1$. We then generate a second uniformly distributed random number that we use to pick one of the four possible nearest-neighbor hops according to their probabilities:

$$\begin{aligned}
P(x_{n,m} \to x_{n+1,m}) &= \frac{\tau^{(1)}_{n,m}}{\tau^{(1)}_{n,m} + \tau^{(2)}_{n,m} + \tau^{(3)}_{n,m} + \tau^{(4)}_{n,m}} \\
P(x_{n,m} \to x_{n-1,m}) &= \frac{\tau^{(2)}_{n,m}}{\tau^{(1)}_{n,m} + \tau^{(2)}_{n,m} + \tau^{(3)}_{n,m} + \tau^{(4)}_{n,m}} \\
P(x_{n,m} \to x_{n,m+1}) &= \frac{\tau^{(3)}_{n,m}}{\tau^{(1)}_{n,m} + \tau^{(2)}_{n,m} + \tau^{(3)}_{n,m} + \tau^{(4)}_{n,m}} \\
P(x_{n,m} \to x_{n,m-1}) &= \frac{\tau^{(4)}_{n,m}}{\tau^{(1)}_{n,m} + \tau^{(2)}_{n,m} + \tau^{(3)}_{n,m} + \tau^{(4)}_{n,m}} \ .
\end{aligned} \tag{27}$$

The particle hops to the new site, and time is incremented by dt.

On a finite lattice with periodic boundary conditions, particles reenter the lattice when they reach the boundaries. Furthermore, the shortest path between two particles may cross the boundary. This is significant, because we are fundamentally interested in the implications of anomalous diffusion for chemical reaction, and the appropriate measure for defining distance between two reactants is the length of the shortest path. We, therefore, define the distance traveled by a diffusing particle as

$$r^2 = \min_{p,q} \left\{ [i - i_0 + pN]^2 + [j - j_0 + qN]^2 \right\} (\Delta r)^2 \ . \tag{28}$$

Here i_0 and j_0 are the initial position coordinates of the particle, N is the dimension of the lattice, and the minimum over integer p and q mathematically defines the shortest path.

An important component of the simulation is the random number generator. A desirable generator ensures that the correct random statistics are used in lattice creation, choice of initial particle positions, choice of hoping directions, and generation of time increments. In this study, we used two random number generators: one that is a sum of three linear congruential generators [29] and an exclusive-or, linear-feedback shift-register method [30]. Unless specified otherwise, all the data that are shown were generated using the sum of three linear congruential generator method.

4. RESULTS

We are interested in the long time diffusive behavior of the particles diffusing on the disordered lattice. Since the diffusion is anomalous, the slope of $\ln\langle r^2 \rangle$ *versus* $\ln t$ will not be unity. This slope will approach 0 as the strength of disorder goes to ∞ and will approach 1 as the strength of disorder goes to 0. We, therefore, examine disorder strengths of varying magnitudes. We find that values of $\beta^2\gamma$ in the range of 1 to 20 produce convincing and high quality results. For $\beta^2\gamma$ too small, the slope will be $1-\varepsilon$, with ε smaller than the noise in our simulation, making the anomalous diffusion difficult to observe. When $\beta^2\gamma$ is too large, strong fluctuations in the particle behavior appear at short times because of significant lattice effects. Within the chosen range of $\beta^2\gamma$, we observe well behaved curves that exhibit distinct disorder strength dependent slopes.

We perform several simulations with different initial starting positions for the random walker. We collect these data as histograms of $\langle r^2(t) \rangle$ *versus* t, with a temporal bin width of $t_0 = 1$. When plotted on a logarithmic scale, these histograms will have much more data for large $\ln(t/t_0)$ than for small $\ln(t/t_0)$. In order to counteract this effect, we use an exponential sequence for selecting data from the histogram when performing the fit to determine the slope. Data for both short times, when the diffusion is not yet anomalous, and long times, when finite size effects are significant, was not used in the fitting procedure. This procedure leads to widely spaced, independent data points. A convenient byproduct of this procedure is that the standard error of the fit gives a reliable estimate of the error in the measured δ. These error bars are included in all of the figures. Note that there could also be a systematic error in each simulation related to the fact that only a single realization of

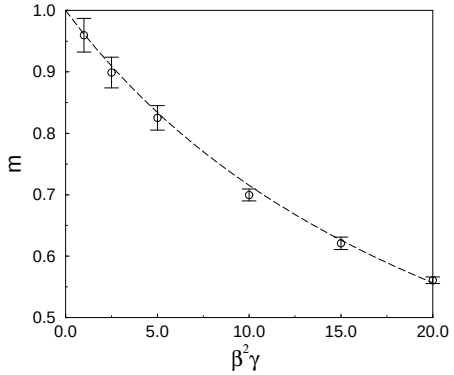

FIG. 1. Shown are the Monte Carlo results for the slope of the mean square displacement, m, as a function of strength of disorder, $\beta^2\gamma$. We have used Eq. (5) to generate the lattice and we placed the random walker uniformly and randomly at the beginning of each random walk. Shown in dashed are the renormalization group predictions.

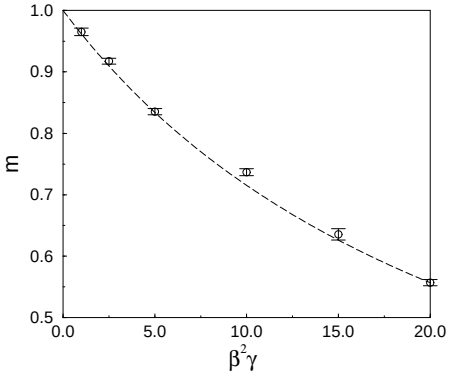

FIG. 2. The same quantities as in Figure 1, but using Eq. (13) to generate the random potential lattice.

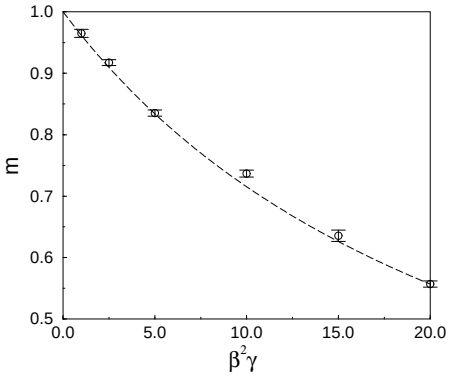

FIG. 3. The same quantities as in Figure 1, except that we have placed the random walker randomly according to a Boltzmann distribution at the beginning of each random walk.

the disorder is employed. This systematic error seems to be small, as simulations with different realizations of the disorder lead to values of δ that differ approximately by the standard error of the fit.

We pick enough different starting positions and follow each simulation long enough to ensure adequate statistics. We found that $N_{do} = 10000$ particles is sufficient to produce fairly smooth histograms for the mean square displacement. We also found that $N_{len} = 2000000$ steps in each random walk is enough for the particles to reach the asymptotic scaling regime. We found that a lattice of size $N = 2048$ is sufficient to give results that span a broad range of times in the scaling regime. In all simulations, the lattice spacing Δr is set equal to unity, which we can enforce by a spatial rescaling. We also set the bare diffusivity equal to unity, which we can similarly enforce by a temporal rescaling. These rescalings will not affect the scaling behavior at long times. The value of δ observed at long times, for example, is independent of these bare values.

Figure 1 shows the slopes determined from simulations with strengths of disorder $1 \leq \beta^2\gamma \leq 20$. We have used Eq. (5) to create the lattice in these simulations. We have chosen the initial position of the random walker uniformly on the lattice, in direct correspondence to the case considered by the renormalization group studies. The data points represent slopes of the mean square travel distances of the random walkers as a function of time. We calculated these values by fitting $\log\langle r^2(t)/(\Delta r)^2\rangle$ as a function of $\ln(t/t_0)$, as described above. For each value of the disorder strength, three independent runs were performed on different realizations of the disorder. We show in Figure 1 the average slope (circles) and the associated standard error of the fit (error bars) for each strength of disorder. The renormalization group predictions are shown as the dashed line. We see excellent agreement between the simulation results and the theoretical predictions, with nearly all the observed values within one standard deviation of the expected value. The varying standard deviations reflect randomness in the potential fields, initial positions, and hopping rates. The slopes do not include contributions from short time behavior or long distance behavior [$\langle r^2\rangle$ on the order of $(N\Delta r)^2$]. Both of these regimes exhibit significant lattice effects, effects not considered in the renormalization group studies.

Figure 2 shows similar data derived from lattice potentials constructed from complex fields, Eq. (13). These results should be identical to those of Figure 1. We observe that the average values are, again, consistent with the theoretical predictions. Interestingly, the standard errors are consistently smaller than those of Figure 1.

Figure 3 shows the slopes that result when the particle initial positions are chosen from a Boltzmann distribution. These conditions mimic those of a transient experiment, such as pulsed field gradient NMR, performed on an equilibrated system. We see agreement between the observed values and the renormalization group predictions, indicating that this change in initial conditions is not "relevant" in the technical sense. We do see less

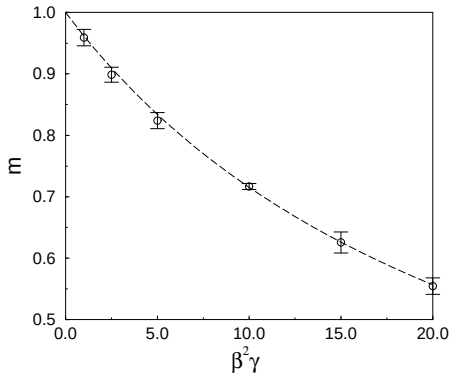

FIG. 4. The same quantities as in Figure 1, but using the the correlation function $\hat{\chi}_{vv}(k) = \gamma \exp(-k^2/2)/k^2$ in creating the random potential.

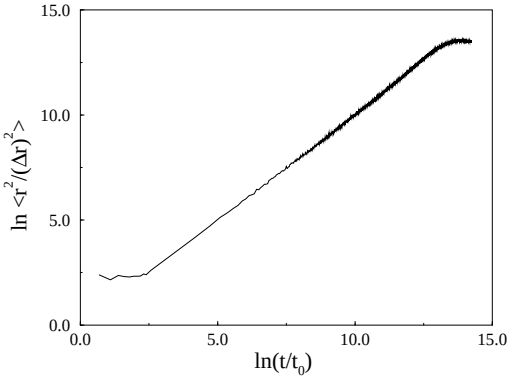

FIG. 5. Shown is the mean square displacement versus time for $\beta^2\gamma = 1$ and $\hat{\chi}_{vv}(k) = \gamma \exp(-k^2/2)/k^2$. We have used Eq. (5) to generate the lattice and we placed the random walker uniformly and randomly at the beginning of each random walk. Note the plateau in the mean square displacement at long times.

consistency in the standard deviations due to the non-uniform sampling of the rugged potential landscape.

Figure 4 shows the slopes that result when one uses the correlation function

$$\hat{\chi}_{vv}(\mathbf{k}) = \gamma \frac{e^{-k^2/2}}{k^2} \ . \tag{29}$$

This correlation function has the same small k behavior as Eq. (1), but distinct behavior for large k. The long-time behavior of these two correlation functions are expected to be the same, as long as $\beta^2\gamma$ is not renormalized by changes in the large k behavior. The prefactor of the mean square displacement, however, is observed to be significantly larger for Eq. (29) than for Eq. (1).

5. DISCUSSION

The results of the computer simulations agree well with the predictions of the renormalization group studies. For each value of $\beta^2\gamma$, the simulations yielded a slope of $\ln\langle r^2/(\Delta r)^2\rangle$ *versus* $\ln(t/t_0)$ in excellent agreement with the analytical predictions. An important observation is that even at long times, $\beta^2\gamma$ does not become renormalized. This is a non-trivial observation, as details in the simulation that are technically "irrelevant" could renormalize $\beta^2\gamma$ a finite amount. For all values of $\beta^2\gamma$, lattice effects produce normal diffusive behavior at short times. This normal diffusion crosses over to anomalous diffusion fairly quickly, within a time corresponding to relatively few hops by the particle. At very long times, the mean square displacement reaches a maximum value due to the periodic boundary conditions. This maximum value is proportional to N^2, since the mean square displacement defined in Eq. (28) is always less than or equal to $(N\Delta r)^2/2$. Figure 5 shows the mean square displacement measured in a typical run. The plateau at long times is clearly visible. The normal diffusion at short times crosses over to anomalous diffusion so rapidly that it is not visible with the histogram bin width we used ($t_0 = 1$).

As discussed, both methods for generating the random lattice potentials, Eq. (5) and (13), lead to Gaussian random fields with the correct correlation function. Both methods should produce the same results for the mean square displacement. We find that, indeed, both approaches give the same average result for the mean square exponent. The real lattice generation is more efficient in terms of memory utilization. One implication of this efficiency, however, is that the real lattice generation is constructed from fewer independent random numbers and is a more severe test of the pseudo-random number generator. The fewer degrees of freedom used when implementing Eq. (3) when compared to Eq. (13) is most likely what leads to the larger error bars in Figure 1 when compared to Figure 2.

The long-range correlations in the random potential allow, in principle, for the possibility that the mean-square displacement depends on the distribution of initial conditions. All of the theoretical predictions, for example, are based upon the assumption of a uniform distribution of initial conditions. In experiments upon equilibrated systems, however, the initial conditions are distributed in a Boltzmann manner. We see from Figure 3 that Boltzmann initial conditions lead to the same mean square exponent at long times.

Two forms of the potential-potential correlation function, Eq. (1) and (29), are used to explore the dependence on irrelevant, large k details. At large distances and long times, the observed scaling behavior that results from the two correlation functions would differ only if technically irrelevant details of the lattice renormalize $\beta^2\gamma$. We found that, indeed, the prefactor of the relation $\langle r^2(t)\rangle \sim at^{1-\delta}$ does depend on these irrelevant details. As we see from Figure 4, however, the exponent is inde-

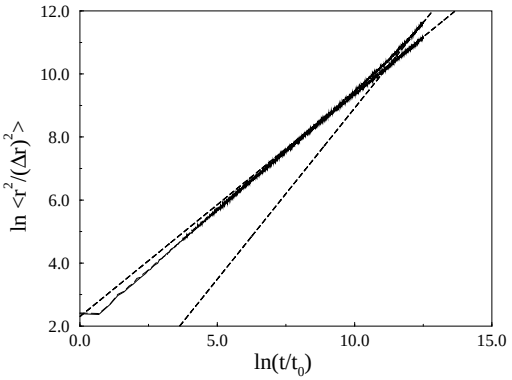

FIG. 6. Shown is the mean square displacement versus time for $\beta^2\gamma = 10$ and $\hat{\chi}_{vv}(k) = \gamma \exp(-k^2/2)/k^2$. We have used Eq. (5) to generate the lattice and we placed the random walker uniformly and randomly at the beginning of each random walk. The top solid curve comes from using the exclusive-or, linear-feedback shift-register pseudo-random number generator [30], and the bottom solid curve comes from the sum of three linear congruential pseudo-random number generators [29]. The bottom curve has the expected slope of $0.71 = 1 - 1/(1 + 8\pi/10)$ at long times. The top curve has a slope of 1.09 at the longest times shown, which indicates superdiffusion. Dashed lines with slopes of 0.71 and 1.09 are shown for convenience.

pendent of these details.

The choice of pseudo-random number generator to use is an important consideration in all Monte Carlo simulations. A pseudo-random number generator is used in three components of the present simulation: in lattice creation, in selecting the particle initial positions, and in creating the transition rates and hop directions. The two random number generators employed in our simulation are a sum of three linear congruential generators [29] and an exclusive-or, linear-feedback-shift register method with table length 55 [30]. Both of these generators are thought to be fairly reliable. All of the results in Figures 1-5 were produced by the sum of three linear congruential generators method. Figure 6 compares the mean square displacements produced by these two generators. The three linear congruential generator method results in slopes for all values of $\beta^2\gamma$ that are consistent with theory. Interestingly, the linear feedback shift register method always leads to slopes greater than expected. Using this generator, one would conclude that $\beta^2\gamma$ is renormalized a finite amount, by some unknown factor. In fact, the factor is the inadequacy of the pseudo-random number generator! At long times, the exponent of the mean square displacement exceeds unity. This super-diffusive behavior is in conflict with a rigorous bound known for diffusion in Gaussian random media: $\lim_{t\to\infty} \langle r^2(t)/t \rangle \leq 4D \exp[-\beta^2 \chi_{vv}(0)]$ [31]. In fact, at long times, this linear feedback shift register method appears to produce ballistic behavior, $\langle r^2(t) \rangle \sim at^2$ (data not shown). This incorrect super-diffusive behavior appears only for potentials that lead to anomalous diffusion. The long-range correlations in the potential, which lead to the anomalous diffusion, apparently couple to the residual correlations in this pseudo-random number generator. Similar, poor results from this type of generator have been observed in another system with long-range correlations—the Ising model at its critical point [32]. In this case, a feedback generator with a short table length led to predicted critical exponents differing from the true values by many times the estimated standard deviation.

6. CONCLUSION

We find a satisfying match between theory and numerical results in our simulation of anomalous diffusion. We found that anomalous behavior occurs in the long time regime, with a transition from normal diffusion at short times. We find that the prefactor for the scaling of the mean square displacement is renormalized by short-distance correlations in the potential, although the exponent is not. Reasonable distributions for the initial conditions lead to the same exponent for the mean square displacement. Interestingly, the correct anomalous diffusion behavior is observed only with a high quality pseudo-random number generator.

ACKNOWLEDGMENTS

This research was supported by the National Science Foundation through grants CHE–9705165 and CTS–9702403.

[1] D. S. Fisher, M. P. A. Fisher, and D. A. Huse, Phys. Rev. B **43**, 130 (1991).
[2] V. E. Kravtsov, I. V. Lerner, and V. I. Yudson, J. Phys. A **18**, L703 (1985).
[3] V. E. Kravtsov, I. V. Lerner, and V. I. Yudson, Phys. Lett. A **119**, 203 (1986).
[4] J. P. Bouchaud, A. Comtet, A. Georges, and P. L. Doussal, J. Physique **48**, 1445 (1987), ; **49**, 369 (1988).
[5] J. Honkonen, Y. M. Pis'mak, and A. V. Vasil'ev, J. Phys. A **21**, L835 (1988).
[6] J. Honkonen and Y. M. Pis'mak, J. Phys. A **22**, L899 (1989).
[7] S. É. Derkachov, J. Honkonen, and Y. M. Pis'mak, J. Phys. A **23**, L735 (1990).
[8] S. É. Derkachov, J. Honkonen, and Y. M. Pis'mak, J. Phys. A **23**, 5563 (1990).
[9] L. Pautmeier, R. Richert, and H. Bässler, Phil. Mag. B **63**, 587 (1991).

[10] A. B. Mosler and E. S. G. Shaqfeh, Phys. Fluids **9**, 1222 (1997).
[11] D. S. Dean, I. T. Drummond, and R. R. Horgan, J. Phys. A **27**, 5135 (1994).
[12] J. F. W. Elliott and A. J. Majda, J. Comput. Phys. **113**, 82 (1994).
[13] J. F. W. Elliott, D. J. Horntrop, and A. J. Majda, J. Comput. Phys. **132**, 384 (1997).
[14] S. Havlin and D. B. Avram, Adv. Phys. **36**, 695 (1987).
[15] M. B. Isichenko, Rev. Mod. Phys. **64**, 961 (1990).
[16] S. Marksteiner, K. Ellinger, and P. Zoller, Phys. Rev. A **53**, 3409 (1996).
[17] R. Bausch, R. Schmitz, and L. A. Turski, Phys. Rev. Lett. **73**, 2382 (1994).
[18] J. P. Bouchaud and A. Georges, Phys. Rep. **195**, 127 (1990).
[19] L. Peliti, J. Phys. A **19**, L365 (1986).
[20] B. P. Lee and J. Cardy, J. Stat. Phys. **80**, 971 (1995); **87**, 951 (1997).
[21] J.-M. Park and M. W. Deem, Phys. Rev. E **57**, 3618 (1998).
[22] M. W. Deem and J.-M. Park, Phys. Rev. E **57**, 2681 (1998).
[23] J.-M. Park and M. W. Deem, Phys. Rev. E **58**, to appear (1998).
[24] M. Deem and D. Chandler, J. Stat. Phys. **76**, 911 (1994).
[25] D. R. Nelson, in *Phase Transitions and Critical Phenomena*, edited by C. Domb and J. Lebowitz (Academic Press, New York, 1983), Vol. 7.
[26] J. P. Bouchaud, A. Comtet, A. Georges, and P. L. Doussal, J. Phys **49**, 369 (1988).
[27] W. H. Press, B. P. Flannery, S. A. Teukolsky, and W. T. Vetterling, *Numerical Recipes in Fortran*, 2nd ed. (Cambridge University Press, New York, 1992).
[28] T. Elston and C. Doering, J. Stat. Phys. **83**, 359 (1996).
[29] B. Wichmann and D. Hill, Byte **12**, 127 (1987).
[30] D. E. Knuth, *The Art of Computer Programming. Volume 2: Seminumerical Algorithms* (Addison-Wesley, Reading, MA, 1981).
[31] A. de Masi, P. A. Ferrari, S. Goldstein, and W. Wick, J. Stat. Phys. **55**, 787 (1989).
[32] A. M. Ferrenberg, D. Landau, and Y. J. Wong, Phys. Rev. Lett. **69**, 3382 (1992).